

Angular momentum variation of the Milky Way thick disk: The dependence of chemical abundance and the evidence on inside-out formation scenario

GUOZHEN HU (胡国真)^{1,2} ZHENGYI SHAO (邵正义)^{1,3} AND LU LI (李璐)^{1,2}

¹Key Laboratory for Research in Galaxies and Cosmology, Shanghai Astronomical Observatory, Chinese Academy of Sciences, 80 Nandan Road, Shanghai 200030, China

²University of Chinese Academy of Sciences, 19A Yuquan Road, 100049, Beijing, China

³Key Lab for Astrophysics, Shanghai 200234, China

ABSTRACT

We investigate the angular momentum of mono-abundance populations (MAPs) of the Milky Way thick disk by using a sample of 26,076 giant stars taken from APOGEE DR17 and Gaia EDR3. The vertical and perpendicular angular momentum components, L_Z and L_P , of MAPs in narrow bins have significant variations across the $[\alpha/M]$ - $[M/H]$ plane. L_Z and L_P systematically change with $[M/H]$ and $[\alpha/M]$ and can be alternatively quantified by the chemical gradients: $d[M/H]/dL_Z = 1.2 \times 10^{-3} \text{ dex kpc}^{-1} \text{ km}^{-1} \text{ s}$, $d[M/H]/dL_P = -5.0 \times 10^{-3} \text{ dex kpc}^{-1} \text{ km}^{-1} \text{ s}$, and $d[\alpha/M]/dL_Z = -3.0 \times 10^{-4} \text{ dex kpc}^{-1} \text{ km}^{-1} \text{ s}$, $d[\alpha/M]/dL_P = 1.2 \times 10^{-3} \text{ dex kpc}^{-1} \text{ km}^{-1} \text{ s}$. These correlations can also be explained as the chemical-dependence of the spatial distribution shape of MAPs. We also exhibit the corresponding age dependence of angular momentum components. Under the assumption that the guiding radius (R_g) is proportional to L_Z , it provides direct observational evidence of the inside-out structure formation scenario of the thick disk, with $dR_g/d\text{Age} = -1.9 \text{ kpc Gyr}^{-1}$. The progressive changes in the disk thickness can be explained by the upside-down formation or/and the consequent kinematical heating.

Keywords: Galaxy: disk — Galaxy: evolution — Galaxy: kinematics and dynamics — Galaxy: structure — methods: data analysis — stars: abundances

1. INTRODUCTION

It is widely accepted that the Milky Way disk consists of two prominent components (Gilmore & Reid 1983), the dynamically hot thick disk and the cold thin disk (e.g., Recio-Blanco et al. 2014; Guiglion et al. 2015; Wojno et al. 2016). In general, the correspondences between stellar ages and spatial distributions (in both radial and vertical senses) indicate that the overall formation of the disk occurred in an inside-out and upside-down manner from the thick disk to the thin disk (Bovy et al. 2012; Bird et al. 2013; Bovy et al. 2016; Freudenburg et al. 2017; Frankel et al. 2019). In this scenario, the older stars formed in an early chaotic bursty mode, with a geometrically thicker layer and a smaller radial scale length, while the younger populations formed in a thin-

ner but radially larger disk.

In focusing on the thick disk, the short formation time scale makes it difficult to investigate how its structure formed. Many simulations proposed that the thick disk formed in an inside-out fashion (e.g., Samland & Gerhard 2003; Schönrich & McMillan 2017; Kawata et al. 2018). **But this formation scenario lacks direct and significant observational evidence.** For instance, by using G-type dwarfs from SDSS/SEGUE, Bovy et al. (2012) found that the scale lengths of the α -enhanced sub-populations (dominated by the thick disk) are all similar, suggesting no inside-out signals. Haywood et al. (2018) claimed three hints against the inside-out scenario, including that the disk scale length does not increase with time, the radial metallicity gradient of the thick disk is flat, and the chemical abundances have very small dispersions at a given age. Recently, Katz et al. (2021) investigated APOGEE DR16 stars in the $[\alpha/\text{Fe}]$ - $[\text{Fe}/\text{H}]$ plane and found that the ridge-lines of

sub-samples with different guiding radii slightly change with the $[\alpha/\text{Fe}]$, which can be regarded as weak evidence of the inside-out formation of the thick disk.

There are two crucial observational aspects in investigating the thick disk structure formation, the stellar initial spatial distribution and the stellar age. Unfortunately, both of these are difficult to obtain.

First, it is a challenge to deduce the spatial distribution of stars at birth from their present-day Galactic radius due to the radial migration (*blurring* and *churning*), which can redistribute the stars and ambiguate the memory of their initial kinematic status (Yu et al. 2012; Vera-Ciro et al. 2014; Toyouchi & Chiba 2014; Jia et al. 2018). *Blurring* is a process in that disk stars move away from their born positions through epicyclic motion (Schönrich & Binney 2009; Sellwood 2014; Holmberg et al. 2009; Aumer & Binney 2009; Mackereth et al. 2019). It conserves the angular momentum of individual stars. The *churning* process may occur through the resonant interaction between stars and the non-axisymmetric structures of the gravitational potential (spirals or bar) (Sellwood & Binney 2002; Solway et al. 2012; Roškar et al. 2012). It changes the angular momentum of individual stars, but for a single population of a given birth radius, this process will increase the dispersion in angular momentum while roughly keeping the average value (see Figure 3 of Sanders & Binney 2016) and does not “heat” the disk radially (Kubryk et al. 2015). **Therefore, using the angular momentum (L) of the stars instead of their Galactic radius may greatly mitigate the problems caused by migration.**

Additionally, the angular momentum is the most fundamental quantity of disk galaxies. It is a better indicator of the disk formation and the gas-infall process (Fall & Romanowsky 2018). The vertical angular momentum component L_z can characterize the radial sense of the disk, and the perpendicular component L_p relates to the thickness of the disk. Overall, the variation of angular momentum of disk stellar populations is essential in recovering the thick disk structure formation process.

Another difficulty is in acquiring accurate stellar age. Current age measurements of individual stars have large uncertainties (Ness et al. 2016) comparable to the short formation timescale of the thick disk, which makes it difficult to intuitively describe the star formation history of the

thick disk. Alternatively, because the gas-infall and star formation processes during the disk structure formation are closely related to chemical enrichment, many studies have used chemical abundance as a proxy of stellar age (e.g. Bovy et al. 2012, 2016; Haywood et al. 2013; Minchev et al. 2017; Feuillet et al. 2019).

Recent works **suggested** employing mono-abundance populations (MAPs). A MAP consists of stars with similar abundance, e.g., metallicity $[M/H]$ and the α -enhancement $[\alpha/M]$ (e.g., Bovy et al. 2012, 2016; Mackereth & Bovy 2020), which are supposed to have a common origin with similar ages and chemical enrichment histories. Usually, MAPs are regarded as mono-age populations, making them physically intuitive indicators of galaxy formation processes (e.g., Bovy et al. 2012, 2016; Minchev et al. 2017).

Therefore, it is worthwhile to investigate the variation of the angular momentum of different MAPs of the thick disk to reveal its structure formation. This paper presents such an investigation based on a large sample of giant stars (Hu & Shao 2022, hereafter HS22) from APOGEE DR17 (Abdurro’uf et al. 2022) and Gaia EDR3 (Gaia Collaboration et al. 2021; Lindegren et al. 2021). We analyze the distribution of orbital parameters of small MAPs of the thick disk, including the angular momentum components and orbital eccentricity, to detect the variation and evolution of these parameters and subsequently discuss their dependence on chemical abundance.

Additionally, although the current stellar age measurements have large uncertainties for individual stars, it is still possible for us to statistically constrain the typical **age of a given MAP**. Then we can directly obtain the correlation between stellar age and angular momentum and recreate the thick disk’s radial and vertical structure formation scenario.

This paper is organized as follows. In the next section, we introduce the thick disk sample and the observational or derived parameters of sample stars. Section 3 shows the results of orbital parameters of MAPs, including the angular momentum components and orbital eccentricity. In Section 4, we first discuss the correlations between angular momentum and chemical abundances and then use the Sanders & Das (2018) catalog of stellar age to debate the dependence of angular momentum with stellar age and finally generalize these relationships to a disk formation scenario. Conclusions are summarized

in Section 5.

2. SAMPLE AND DATA

2.1. Thick disk sample

In HS22, we have identified and quantified four sub-disk components of the Milky Way by using the chemical abundances ($[M/H]$, $[\alpha/M]$) and the 3D velocities (V_R , V_ϕ , V_Z) taken or derived from APOGEE DR17 and Gaia EDR3 for a sample of 119,558 giant stars. We briefly describe the procedure of HS22 below. Firstly, the sample stars were divided into $[M/H]$ bins. For each bin, we used the multivariate Gaussian Mixture model (GMM) to fit the subsample with other four variables, $[\alpha/M]$, V_R , V_ϕ and V_Z . In the range of $-1.2 < [M/H] < 0.4$ dex, all bins were well modeled by two Gaussian components belonging to the high- α or low- α sequences separately. These two sequences were further separated at $[M/H] = -0.1$ dex to denote metal-poor or metal-rich parts. Thus, four sub-disk components were determined and named as $h\alpha mp$, $h\alpha mr$, $l\alpha mp$, and $l\alpha mr$ separately. Of these, the $h\alpha mp$ component, which corresponds to the canonical thick disk, has the hottest kinematics and the smallest radial distribution (see Fig. 2 and 5 of HS22). It is significantly distinguished from the other three sub-disks. In this paper, we follow the work of HS22 and **select** only the thick disk (the $h\alpha mp$ component) for investigation.

We restrict the thick disk sample stars in the region of $-1.0 < [M/H] < -0.1$ dex and $0.15 < [\alpha/M] < 0.35$ dex (the red box in Fig. 1). In this region, there are 26,076 giant stars having good quality of chemical and astrometrical data from APOGEE DR17 and Gaia EDR3. As a by-product of the GMM, we have calculated the membership probabilities for individual stars belonging to each α -sequence (Table 2 of HS22). In this work, we select 24,935 thick disk stars ($\sim 96\%$ stars within the given region) having membership probability $P_{h\alpha} > 0.99$. This choice ensures us that the thick disk sample has very little contamination from other sub-disk components.

2.2. Angular momentum and orbital eccentricity

In HS22, for each sample star, we have calculated the 6D kinematical information (3D positions and 3D velocities) relative to the Sun, by using the coordinates and proper motions from Gaia EDR3, the radial velocities from APOGEE DR17 and the photo-geometric distances estimated by Bailer-Jones et al. (2021). They have been transformed into the Galactocentric cylindri-

cal system (R_{gc} , ϕ , Z , V_R , V_ϕ , V_Z) by assuming that the Galactocentric distance of the Sun is $R_\odot = 8.125$ kpc (GRAVITY Collaboration et al. 2018) and its height from the Galactic plane is $Z_\odot = 20.8$ pc (Bennett & Bovy 2019), and the solar motions are (11.1, 242, 7.25) km s^{-1} in the radial, rotational and vertical directions, respectively (Schönrich et al. 2010; ?). In this work, we subsequently use the 6D kinematic data as the input of the GALPOT package to integrate the stellar orbit of each sample star under the Galactic potential model of McMillan (2017). Thus, we obtain the vertical and perpendicular angular momentum components L_Z and L_P . Additionally, we obtain the Galactic pericenter (r_{peri}) and apocenter (r_{apo}) radii, and then derive the orbital eccentricity defined as $ecc = (r_{apo} - r_{peri}) / (r_{apo} + r_{peri})$.

Usually, the L_Z of star can be transferred to its guiding radius (R_g) based on the relationship $V_\phi^2 / R_g = L_Z^2 / R_g^3$ (Toyouchi & Chiba 2014). We calculate the R_g for each star under the assumption that the rotational velocity is a constant across the region covering our thick disk sample, with $V_\phi = 230 \text{ km s}^{-1}$ (Schönrich et al. 2010; ?). These value-added measurements (L_Z , L_P , ecc and R_g) are listed in Table 1 and its machine-readable form is available.

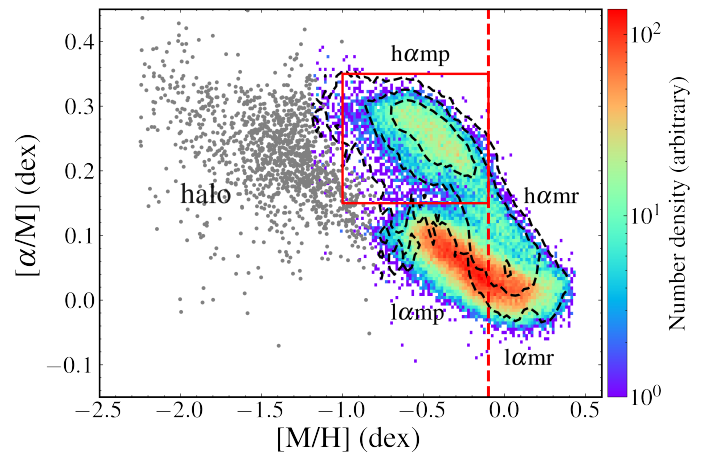


Figure 1. Number density distribution of HS22 sample stars in the $[\alpha/M]$ - $[M/H]$ plane. The colored distribution is for the disk components and black-dashed lines represent the 1 and 2 σ contours for the high- α sequence only. The red dashed vertical line at $[M/H] = -0.1$ dex dividing the metal-poor and metal-rich regions. The red box delineates the canonical thick disk ($h\alpha mp$) region selected for this paper. Halo stars are shown as grey dots.

2.3. Stellar age

Sanders & Das (2018) provided a catalog of stellar parameters, including the stellar age, based on the Bayesian framework inference using broad-band photometric, spectroscopic and astrometric information. This catalog matches our giant star sample to a large extent. **We rejected stars with age uncertainties $\sigma_\tau > 1.5$ Gyr. Our final sample contains 11,761 giant stars having age measurements, which is about 47% of the sample.**

It should be mentioned that Sanders & Das (2018) use a prior on age, metallicity, and position in their Bayesian framework, i.e., stars of the thick disk component tend to be older and more metal-poor than stars of the thin disk component. So the prior is not fully independent between stellar age and metallicity, though it has a very wide distribution on the $[\text{Fe}/\text{H}]$ -age plane. However, we **assume** that the prior of Sanders & Das (2018) is reasonable for the MW components, so the age measurements for individual stars are reliable. They are independent to the angular momentum and should be suitable in subsequent discussion of the angular momentum evolution (cite Sec. 4.2).

3. ANGULAR MOMENTUM AND ORBITAL PROPERTIES ACROSS $[\alpha/\text{M}]-[\text{M}/\text{H}]$ PLANE

We split the stellar sample into mono-abundance bins with bin size of $0.025 \times 0.025 \text{ dex}^2$ for $[\text{M}/\text{H}]$ and $[\alpha/\text{M}]$. This bin size is chosen to be slightly larger than the typical abundance uncertainties of the APOGEE catalog ($0.01 \sim 0.02 \text{ dex}$), but it is small enough to resolve the thick disk region (the red box in the Fig. 1) in the $[\alpha/\text{M}]-[\text{M}/\text{H}]$ plane.

We select the MAPs with the number of star $n > 30$ for investigation. These MAPs cover the dominant part of the thick disk region ($\sim 2\sigma$ of the number density contour in Fig. 2). For parameters that will be discussed in this paper, such as the angular momentum components (L_Z, L_P), the orbital eccentricity (ecc) and the stellar age, we notice that they all have non-negligible dispersions for each MAP due to the intrinsic distributions and/or the observational uncertainties. Nevertheless, we suppose that their median values are statistically robust and could be reasonably adopted to determine the variations across the entire thick disk region. Therefore, in the following context, each MAP's properties are specifically referred to their median values unless otherwise stated. The corresponding dispersions (σ) of parameters for each MAP are quantified in term of half

of the 16% to 84% interval respectively.

In Fig. 2, we plot L_Z, L_P and ecc of MAPs on the $[\alpha/\text{M}]-[\text{M}/\text{H}]$ plane. These parameters show significant variations and systematic changes across the metallicity and the α -enhancement.

Angular momentum: Panels (a) and (c) of Fig.2 plot the color-coded L_Z and L_P values. **Both of these two angular momentum components show significant variations, with L_Z from 800 to 1600 kpc km s^{-1} and L_P from 230 to 450 kpc km s^{-1} .** The L_Z increases/decreases with the metallicity/ α -enhancement and the L_P follows an opposite trend. One can also find that they present monotonous changes along the number-density ridge line (the dotted line in each panel), which represents the well-known chemical abundance evolutionary trajectory (e.g. Spitoni et al. 2019, see their Fig.2; Lian et al. 2020, see their Fig.7). Notably, **the distribution of L_Z** appears to have a horizontal structure in the $[\alpha/\text{M}]-[\text{M}/\text{H}]$ plane, which means that, at a given metallicity, higher- α MAPs tend to have lower L_Z values.

Panels (b) and (d) show the corresponding angular momentum dispersions, σ_{L_Z} and σ_{L_P} . **Both of them** decrease with the metallicity, indicating that MAPs at more metal-poor stage have larger angular momentum dispersions. **This phenomenon could be** mainly due to the *churning* effect, which disperses the angular momentum distributions for a given stellar population.

Orbital eccentricity: It shows a systematic variation of ecc along the evolutionary trajectory, from 0.50 to 0.18, with more metal-poor stars having larger eccentricities (panel (e)). Interestingly, **the distribution of ecc** also has a horizontal structure, which is similar to that of the L_Z in panel (a) but with the opposite trends along the evolutionary trajectory. It implies an anti-correlation between L_Z and ecc of the current sample. Notably, this anti-correlation is partly attributed to the effect of the *blurring* radial migration (e.g., Toyouchi & Chiba 2014; Aumer et al. 2016). Disk stars with larger orbital eccentricities are more probably to be observed around their apocenter points rather than near the pericenter points. So apparently, a solar-centric sample may contain more inner (less L_Z or R_g) stars with more eccentric orbits. This

kind of observational selection bias actually helps us to extend our sample coverage towards the inner part of the MW disk.

Panel (f) shows the corresponding dispersion of orbital eccentricity, **where σ_{ecc} decreases** with the metallicity, indicating that more metal-poor MAPs have larger eccentricity dispersions, which maybe also due to the *blurring* effect for older stellar populations.

In summary, we find that the thick disk MAPs have significant variations of angular momentum and orbital eccentricity across the $[\alpha/M]$ - $[M/H]$ plane, which implies a strong correlation of its formation scenario and chemical evolution.

4. DISCUSSIONS

4.1. Chemical dependence of angular Momentum

If we treat the MAPs as independent observational data points, we can directly detect the correlations between chemical abundances ($[M/H]$ or $[\alpha/M]$) and angular momentum components (L_Z or L_P). Since L_Z or L_P is closely related to the radial scale or thickness of the disk, these two correlation slopes can be regarded as substitutes for the radial and vertical gradients of chemical abundances.

4.1.1. L_Z and radial gradients of chemical abundances

The correlation between $[M/H]$ and L_Z is **visible** in panel (a) of Fig. 3, with the slope of $d[M/H]/dL_Z = 1.2 \times 10^{-3} \text{ dex kpc}^{-1} \text{ km}^{-1} \text{ s}$, or $d[M/H]/dR_g = 0.28 \text{ dex kpc}^{-1}$. **It indicates the inverse L_Z or radial gradients of $[M/H]$, suggesting that the stars born in the outer part of the thick disk, which exhibit larger L_Z (or R_g), are more metal-rich than those in the inner part.** This correlation is opposite to the overall radial gradient of the MW disk, which declares that the outer (thin) disk is more metal-poor than the inner (thick) disk, but it supports the model predictions of chemical radial gradient for the individually considered thick disk (Schönrich & McMillan 2017).

We notice that there is a large scatter of the $[M/H]$ - L_Z correlation, which is mainly due to the different $[\alpha/M]$ values. For MAPs with a given $[M/H]$, e.g. $[M/H] \sim -0.5$, the $[\alpha/M]$ significantly decrease with L_Z

(or R_g) (shown as the changes of color in panel (a) of Fig. 3). These MAPs have the same $[M/H]$ but different α -enhancement, which implies that they have different chemical-enrichment processes. **It agrees that, in the inner region of the thick disk, stars formed in a denser gas environment may have a higher star formation rate leading to a more rapid α -enhancement (e.g., Haywood et al. 2016).**

The L_Z dependence of $[\alpha/M]$ is also shown as a tight relationship between $[\alpha/M]$ and L_Z (or R_g), where the smaller L_Z (or R_g) MAPs have larger $[\alpha/M]$ values (panel (c) of Fig. 3). Despite the $[\alpha/M]$ - L_Z correlation **is not linear in this work**, we estimate the overall slope of $d[\alpha/M]/dL_Z = -3.0 \times 10^{-4} \text{ dex kpc}^{-1} \text{ km}^{-1} \text{ s}$, alternatively $d[\alpha/M]/dR_g = -0.07 \text{ dex kpc}^{-1}$, which claims a significant L_Z or radial gradient of $[\alpha/M]$. **The $[\alpha/M]$ - L_Z (R_g) correlation is consistent with the findings of Katz et al. (2021), who analyzed the giant stars of the thick disk from APOGEE DR16. Their work compared the ridge lines in the $[\alpha/Fe]$ - $[Fe/H]$ plane for sub-samples with varying R_g and found the inner stars having higher $[\alpha/Fe]$ positions.**

The radial gradients of chemical abundances of the thick disk have been explored in many previous works (e.g., Carrell et al. 2012; Mikolaitis et al. 2014; Li et al. 2018). Most of them reported weak or none gradients. Probably, that is because they have only use the current Galactocentric distance R_{gc} of the sample star while the radial migration throughout the disk may eliminate the radial metallicity gradient (Li et al. 2018). In this work, we employ the guiding radius (R_g), or the vertical angular momentum (L_Z), which can avoid the *blurring* migration effect for individual stars and also make the *churning* effect negligible for the MAPs. So, the MAPs' average properties **describe** the original condition of thick disk at most and the initial radial gradients can be more easily exhibited.

4.1.2. L_P and vertical gradients of chemical abundances

Panels (b) and (d) of Fig. 3 show the significant chemical- L_P correlations of MAPs. **Firstly**, there is a L_P gradient of metallicity with $d[M/H]/dL_P = -5.0 \times 10^{-3} \text{ dex kpc}^{-1} \text{ km}^{-1} \text{ s}$. Considering the L_P uncertainties are quite large (typically shown as the error bar in panel (b)), the $[M/H]$ - L_P correlation should be extremely tight with very small internal scatters. **Secondly**, the correlation between $[\alpha/M]$ and L_P is also significant (in panel (d)) but with a much larger scat-

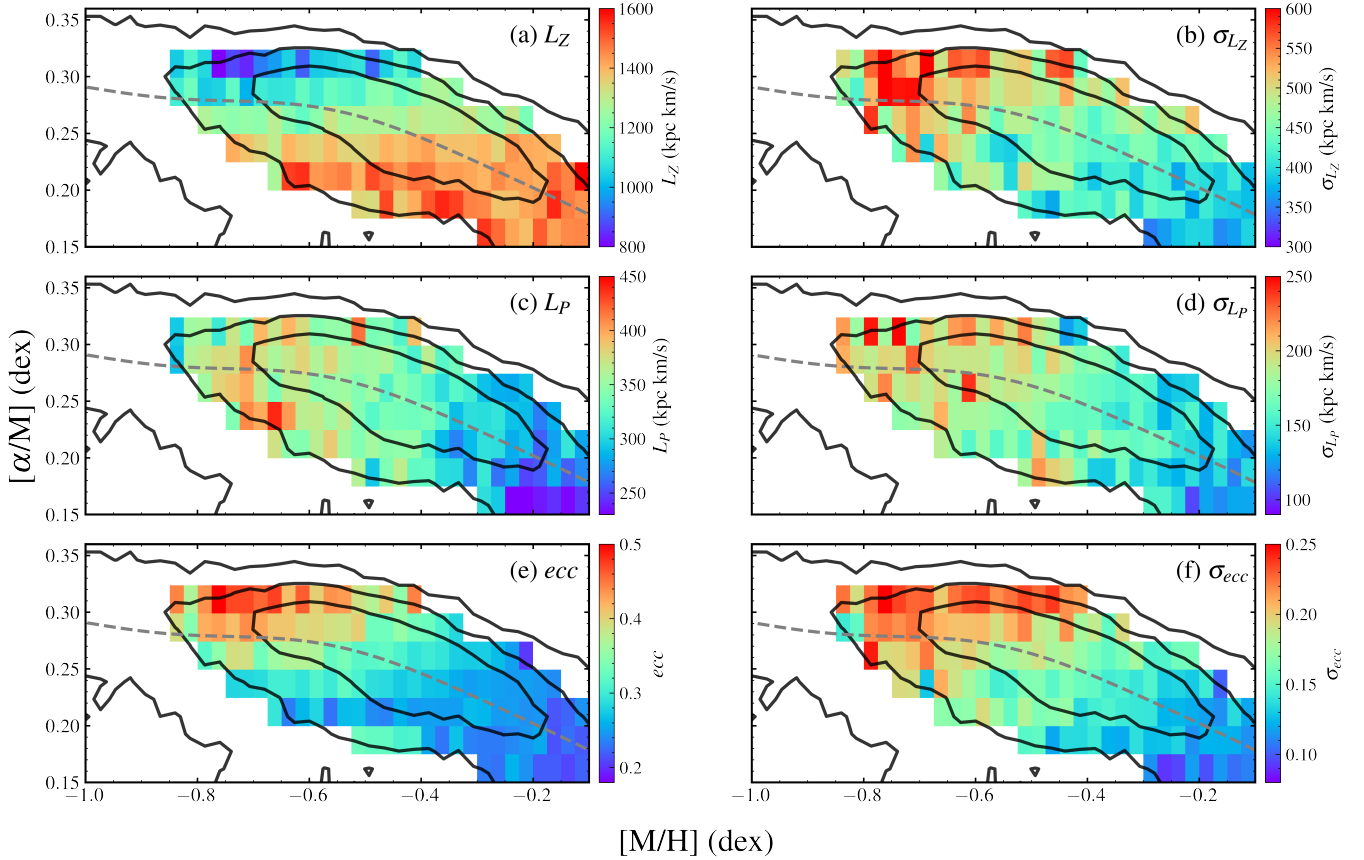


Figure 2. Distributions of the MAP's parameters in the $[\alpha/M]$ - $[M/H]$ plane. Parameters are coded by color, including L_Z , L_P , ecc and the dispersions σ_{L_Z} , σ_{L_P} and σ_{ecc} , respectively. The black lines represent 1σ , 2σ and 3σ contours of the number-density distribution of the thick disk sample star. The grey dashed line curves the ridge-line of the number density, which is identified by a robust Gaussian process (Li et al. 2021).

ter than the typical uncertainty of L_P . The slope is $[\alpha/M]/dL_P = 1.2 \times 10^{-3} \text{ dex kpc}^{-1} \text{ km}^{-1}$, indicating an inverse L_P gradient of $[\alpha/M]$. Moreover, we can find that the scatter is mainly due to the different $[M/H]$ values, which can be regarded as the conditional $[M/H]$ - L_P correlation at given $[\alpha/M]$. Therefore, we conclude that the $[M/H]$ - L_P correlation dominates the relationship among these three parameters.

Since the L_P value decides the height from the Galactic plane of a star can reach, Z_{\max} , the chemical dependencies on L_P then correspond to the vertical gradients of chemical abundance. **That means, for our thick disk sample, the thinner distributed populations (with smaller L_P) have more metal-richness and less α -enhancement.** Previous works reported weak vertical gradients when the current height value $|Z|$ is used as diagnostics (e.g., Li et al. 2018; Yan et al. 2019). **We suggest** that the L_P gradients of chemical abundances are intrinsic features of the thick disk due to its formation, and the use of $|Z|$ weakens this phe-

nomenon.

Moreover, if MAPs with larger L_P values are expected to have larger vertical velocity dispersions (σ_{V_Z}), the chemical dependence of L_P will also be reflected as the chemical- σ_{V_Z} relationships, which has been already shown in previous works. For example, HS22 reported that, σ_{V_Z} of the thick disk (the hamp disk) monotonously decreases with $[M/H]$ from 71 to 31 km s^{-1} by using the same giant star sample of this paper. Haywood et al. (2013) found that σ_{V_Z} progressively decreases with the decreasing of $[\alpha/\text{Fe}]$ from about 50 to 25 km s^{-1} for a sample of thick disk dwarf stars (see their Fig.11), suggesting that the star formation proceeded in progressively thinner layers.

4.2. Age dependent angular momentum

The star-forming process **leads** to a sustained metallicity enrichment, accompanied by a decrease in the α -enhancement. Therefore, the change of chemical abundance in forming stellar populations is usually re-

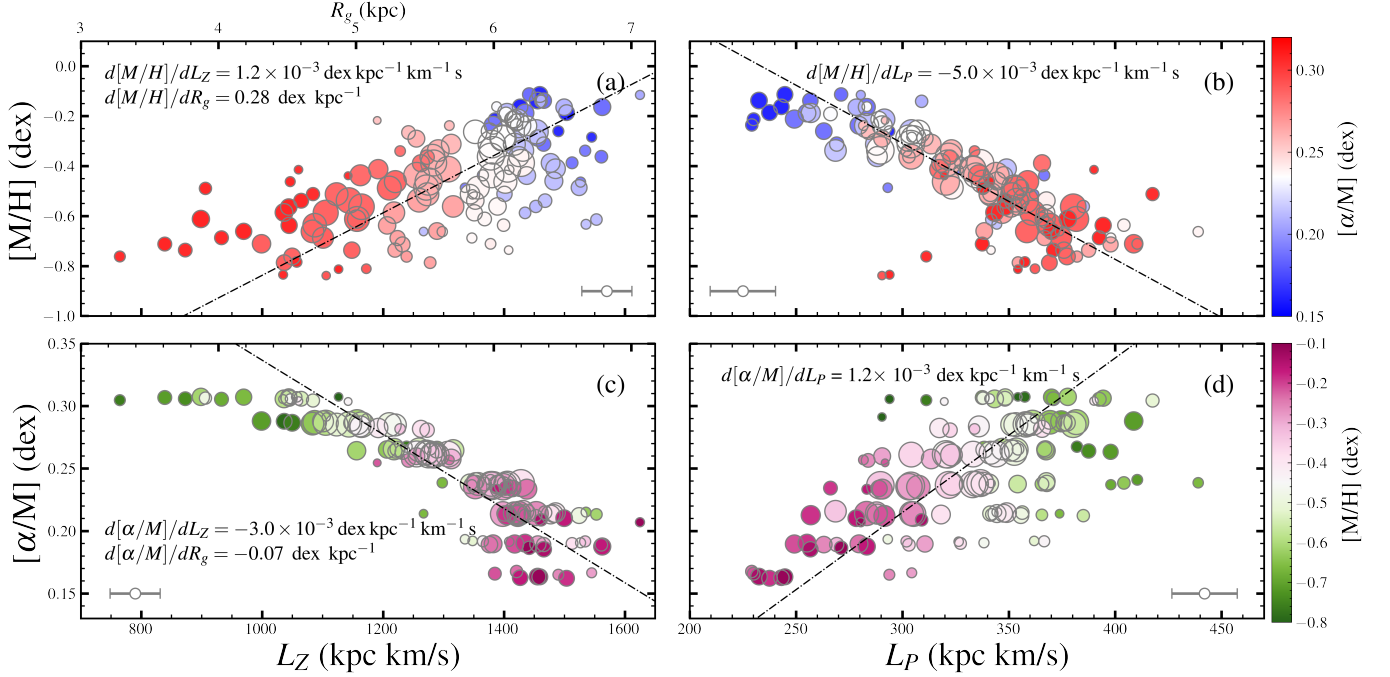


Figure 3. Correlations between chemical abundance and angular momentum of MAPs. Top panels: for the $[M/H]$; Bottom panels: for the $[\alpha/M]$. Different angular momentum components, L_Z (or R_g) and L_P are plotted on the left and right panels, respectively. The symbol size represents the star number n of MAP, from 33 to 428. The symbol color are coded by the median values of $[\alpha/M]$ for the top panels, and $[M/H]$ for the bottom panels. The error bars in the corner of each panel represent the typical uncertainties of the median values of corresponding parameters, which is estimated as σ/\sqrt{n} . The slopes of each correlation (dash-dotted lines) are fitted linearly with the uncertainties of median value to be taken into account.

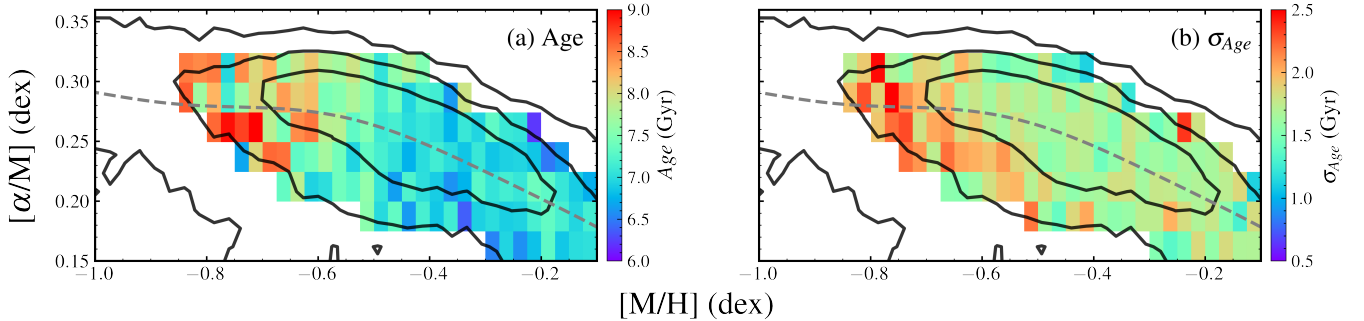


Figure 4. Distributions of the MAP's stellar age (panel (a)) and the dispersions σ_{Age} (panel (b)) in the $[\alpha/M]$ - $[M/H]$ plane. The contour and dash line are the same as in Fig.2.

garded as an indication of time. So the corresponding changes of the angular momentum components with the chemical abundance can be considered as the structure evolution (Bovy et al. 2012; Bird et al. 2013; Bovy et al. 2016). Nevertheless, the direct correlation between stellar age and angular momentum is still expected to explore the structure formation process intuitively.

We employ the stellar age measurements of the Sanders & Das (2018) catalog, and plot the age of MAPs across the $[\alpha/M]$ - $[M/H]$ plane in Fig.4. The median ages of MAPs vary from 6.0 to 9.0 Gyr (panel

(a)). The σ_{Age} of MAPs are slightly different, with older MAPs having larger age dispersion (panel (b)). If we estimate the uncertainty of the median value as σ_{Age}/\sqrt{n} , then the errors are from 0.11 to 0.60 Gyr, with a typical value of ~ 0.25 Gyr. **The age variation of MAP follows the trajectory of chemical enrichment. More metal-poor or more high- α MAPs exhibiting larger stellar ages, which reflects that the age dependence of chemical abundances of the thick disk is substantial.** It reveals the process of chemical evolution, though the thick disk is believed to have a **bursty** star formation. This result confirms

previous works, which point out the tight age-[M/H] or age-[α /M] correlations of the thick disk (e.g., Haywood et al. 2013; Minchev et al. 2017).

Similarly, by using MAPs as **observational data points**, we can directly investigate the correlation between the age and angular momentum. As shown in **panel (a)** of Fig. 5, the L_Z of MAP decreases substantially with stellar age, having $dL_Z/d\text{Age} = -435.7 \text{ kpc km s}^{-1} \text{ Gyr}^{-1}$. This slope corresponds to $dR_g/d\text{Age} = -1.9 \text{ kpc Gyr}^{-1}$ alternatively. We claim that such a steep slope is strong evidence of the radial enlargement of the thick disk.

As a comparison, we plot the current Galactic radius R_{gc} vs age in panel (b) of Fig. 5. The correlation is also significant, but the dependence is very weak with $dR_{gc}/d\text{Age} = -0.24 \text{ kpc Gyr}^{-1}$. Generally, R_{gc} is larger than R_g for all MAPs with different increments according to their ecc values. It is just the impact of the *blurring* radial migration. MAPs with more eccentric orbits can move further than their birthing places ($\sim R_g$) and tend to be observed near their apocentre. That is why many works found no (or only slight) enlargement of the thick disk radial size if they only used the R_{gc} for diagnosing (Bovy et al. 2012, 2016). In other words, it is difficult to detect the inside-out feature of the thick disk formation because the stars are no longer located where they were born due to the radial migration.

Panel (c) of Fig. 5 shows the correlation between L_P and age, with younger MAPs having smaller L_P values and $dL_P/d\text{Age} = 112.4 \text{ kpc km s}^{-1} \text{ Gyr}^{-1}$. This correlation exhibits the phenomenon that the spatial distributions of stars in younger MAPs formed in thinner layers, or the older MAPs were getting thicker after star formation.

4.3. Structure formation scenario of the thick disk

Combining all the angular momentum correlations discussed in sections 4.1 and 4.2, we have solid observational evidence for the thick disk formation. Older (or relatively metal-poor/high- α) stellar populations have smaller and thicker spatial distribution than younger (or relatively metal-rich/low- α) populations.

This phenomenon constrains the structure formation process and can be well explained by an inside-out and upside-down scenario. It starts with a major in-fall of metal-poor gas. The gas with smaller angular

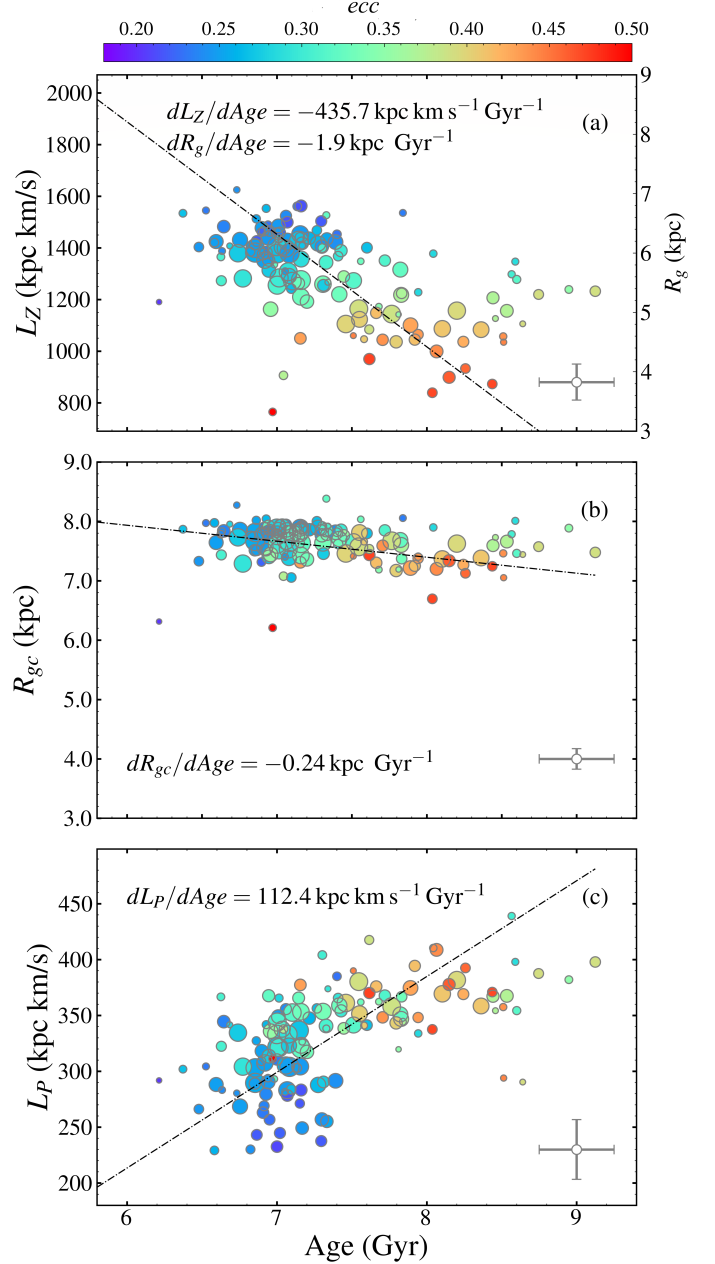


Figure 5. Correlations between MAP's parameters and stellar age. L_Z (or R_g), R_{gc} and L_P are plotted in separate panels, with each symbol representing a MAP. The color is coded by the median value of ecc . The symbols with error bars in the corners of each panel represent the typical uncertainties of the median values of corresponding parameters. The slopes of each correlation (dash-dotted lines) are fitted using the orthogonal distance regression, and the uncertainties of the median values are taken into account. (<https://docs.scipy.org/doc/scipy/reference/odr.html>)

momentum **first** cooled down and ignited the starburst formation process. The dense inner region caused a higher star-forming rate (SFR), so these populations are relatively more metal-poor but have higher α -enhancement. The larger angular momentum gas subsequently inflowed and cooled down into the outer region. The outer gas may be enriched by the previous star formation and a lower SFR is required to occur the lower α -enhancement. Meanwhile, it provides sufficient cooling time to form the larger but thinner-distributed stellar populations. This scenario confirms the model or simulation predictions. For instance, [Kawata et al. \(2018\)](#) performed N-body simulations and suggested that the thick disk was built-up in an inside-out and upside-down fashion, with older, smaller, and thicker populations being more metal-poor (see their Fig. 1).

Alternatively, kinematic heating is another effective mechanism that can thicken the older populations if they are formed from a relatively flat disk ([Schönrich & McMillan 2017](#)). **Actually, the observational evidence presented in this paper cannot clearly distinguish these two mechanisms. They may co-exist, which means the disk settles over time in an 'upside-down' formation scenario,** and the stellar populations are heated up after birth ([Bird et al. 2021](#)).

Now we can summarize the structure formation history of the entire MW disk as a **hierarchically inside-out formation process**. The first stage is about the inside-out formation of the thick disk, which is claimed in this paper. The second stage is the consequently inside-out formation procedure of inner disk components, from the canonical thick (hamp) disk to the hamr disk and then to the lomr disk (see HS22 for details). Finally, the third stage is the overall formation sequence from the thick (inner) disks to the thin (outer) disk shown in previous works (e.g., [Brook et al. 2006](#); [Bird et al. 2013](#); [Minchev et al. 2015](#)). However, it is worth noting that these similar structure formation patterns occur in opposite chemical radial gradients, indicating that they actually have different origins. The canonical thick disk formed earlier from highly turbulent gas. It quickly enriched the latter star formation region (with larger L_Z or R_g) of the thick disk so that it caused an inverse $[M/H]$ gradient. In contrast, the canonical thin disk formed mainly due to the second gas accretion of the MW so that the outer disk region was continually rejuvenated by lower- $[M/H]$ gas resulting in the gradual decrease of the average stel-

lar metallicity ([Lian et al. 2020](#)).

5. CONCLUSION

Benefiting from the precise 6D kinematics provided by **Gaia EDR3 and APOGEE DR17**, we can get the angular momentum and other orbital properties of the thick disk giant stars. Combining with the chemical abundances from the APOGEE and stellar ages derived from [Sanders & Das \(2018\)](#), we investigate the angular momentum of MAPs and their correlation with chemicals and stellar age. We summarize our main results as follows.

(1) The angular momentum components, L_Z and L_P , of MAPs have significant variations across the $[\alpha/M]$ - $[M/H]$ plane that follow the chemical evolutionary trajectory of the thick disk stellar populations.

(2) These variations are well quantified by the inverse L_Z (or radial) gradient and the L_P (or vertical) gradient of the metallicity ($[M/H]$), and the corresponding correlations between angular momentum components and the α -enhancement ($[\alpha/M]$). The stars of metal-poor (or high- α) MAPs have smaller and thicker distributions than those of metal-rich (or low- α) MAPs.

(3) **The angular momentum components show significant age dependence.** It clearly suggests an inside-out structure formation scenario of the thick disk, which supports the infalling gas going through a gradually extending and cooling down process.

These results provide improved observational constraints on the chemical-spatial distribution of thick disk stars, which calls for rigorous and global chemical-evolution models leading to the angular momentum and chemical **correlations shown** in this paper.

We sincerely thank the anonymous referee for valuable comments and suggestion. This work is supported by the National Natural Science Foundation of China (NSFC) under grants U2031139 and 12273091, the National Key R&D Program of China No. 2019YFA0405501, and the science research grants from the China Manned Space Project with NO. CMS-CSST-2021-A08. This work has made use of data from the European Space Agency (ESA) mission Gaia (<https://www.cosmos.esa.int/gaia>), processed by the Gaia Data Processing and Analysis Consortium (DPAC; <https://www.cosmos.esa.int/web/gaia/dpac/consortium>). Funding for the DPAC has been provided by na-

tional institutions, in particular the institutions participating in the Gaia Multilateral Agreement. The stellar parameters, abundances, RVs from APOGEE DR17 were derived from the allStar files available at <https://www.sdss.org/dr17/>. Funding for the Sloan

Digital Sky Survey IV has been provided by the Alfred P. Sloan Foundation, the U.S. Department of Energy Office of Science, and the Participating Institutions.

Software: Astropy (Astropy Collaboration et al. 2013), Numpy (van der Walt et al. 2011), Scipy (Oliphant 2007), Matplotlib (Hunter 2007).

REFERENCES

- Gilmore, G. & Reid, N. 1983, MNRAS, 202, 1025.
doi:10.1093/mnras/202.4.1025
- Bovy, J., Rix, H.-W., Liu, C., et al. 2012, ApJ, 753, 148.
doi:10.1088/0004-637X/753/2/148
- Brook, C. B., Kawata, D., Martel, H., et al. 2006, ApJ, 639, 126. doi:10.1086/499154
- Minchev, I., Martig, M., Streich, D., et al. 2015, ApJL, 804, L9. doi:10.1088/2041-8205/804/1/L9
- Bird, J. C., Kazantzidis, S., Weinberg, D. H., et al. 2013, ApJ, 773, 43. doi:10.1088/0004-637X/773/1/43
- Bovy, J., Rix, H.-W., Schlafly, E. F., et al. 2016, ApJ, 823, 30. doi:10.3847/0004-637X/823/1/30
- Freudenburg, J. K. C., Weinberg, D. H., Hayden, M. R., et al. 2017, ApJ, 849, 17. doi:10.3847/1538-4357/aa8c03
- Frankel, N., Sanders, J., Rix, H.-W., et al. 2019, ApJ, 884, 99. doi:10.3847/1538-4357/ab4254
- Samland, M. & Gerhard, O. E. 2003, A&A, 399, 961.
doi:10.1051/0004-6361:20021842
- Schönrich, R. & McMillan, P. J. 2017, MNRAS, 467, 1154.
doi:10.1093/mnras/stx093
- Kawata, D., Allende Prieto, C., Brook, C. B., et al. 2018, MNRAS, 473, 867. doi:10.1093/mnras/stx2464
- Katz, D., Gómez, A., Haywood, M., et al. 2021, A&A, 655, A111. doi:10.1051/0004-6361/202140453
- Haywood, M., Di Matteo, P., Lehnert, M., et al. 2018, A&A, 618, A78. doi:10.1051/0004-6361/201731363
- Yu, J., Sellwood, J. A., Pryor, C., et al. 2012, ApJ, 754, 124. doi:10.1088/0004-637X/754/2/124
- Vera-Ciro, C., D’Onghia, E., Navarro, J., et al. 2014, ApJ, 794, 173. doi:10.1088/0004-637X/794/2/173
- Abdurro’uf, Accetta, K., Aerts, C., et al. 2022, ApJS, 259, 35. doi:10.3847/1538-4365/ac4414
- Astropy Collaboration, Robitaille, T. P., Tollerud, E. J., et al. 2013, A&A, 558, A33.
doi:10.1051/0004-6361/201322068
- Bailer-Jones, C. A. L., Rybizki, J., Fouesneau, M., et al. 2021, AJ, 161, 147. doi:10.3847/1538-3881/abd806
- Bennett, M. & Bovy, J. 2019, MNRAS, 482, 1417.
doi:10.1093/mnras/sty2813
- Bird, J. C., Loebman, S. R., Weinberg, D. H., et al. 2021, MNRAS, 503, 1815. doi:10.1093/mnras/stab289
- Bovy, J., Rix, H.-W., & Hogg, D. W. 2012, ApJ, 751, 131.
doi:10.1088/0004-637X/751/2/131
- Carrell, K., Chen, Y., & Zhao, G. 2012, AJ, 144, 185.
doi:10.1088/0004-6256/144/6/185
- Fall, S. M. & Romanowsky, A. J. 2018, ApJ, 868, 133.
doi:10.3847/1538-4357/aac27
- Feuillet, D. K., Frankel, N., Lind, K., et al. 2019, MNRAS, 489, 1742. doi:10.1093/mnras/stz2221
- Sanders, J. L. & Das, P. 2018, MNRAS, 481, 4093.
doi:10.1093/mnras/sty2490
- Li, C., Zhao, G., Zhai, M., et al. 2018, ApJ, 860, 53.
doi:10.3847/1538-4357/aac50f
- Li, Z.-Z., Li, L., & Shao, Z. 2021, Astronomy and Computing, 36, 100483. doi:10.1016/j.ascom.2021.100483
- Jia, Y., Chen, Y., Zhao, G., et al. 2018, ApJ, 863, 93.
doi:10.3847/1538-4357/aad3bb
- Recio-Blanco, A., de Laverny, P., Kordopatis, G., et al. 2014, A&A, 567, A5. doi:10.1051/0004-6361/201322944
- Guiglion, G., Recio-Blanco, A., de Laverny, P., et al. 2015, A&A, 583, A91. doi:10.1051/0004-6361/201525883
- Wojno, J., Kordopatis, G., Steinmetz, M., et al. 2016, MNRAS, 461, 4246. doi:10.1093/mnras/stw1633
- GRAVITY Collaboration, Abuter, R., Amorim, A., et al. 2018, A&A, 615, L15. doi:10.1051/0004-6361/201833718
- Kubryk, M., Prantzos, N., & Athanassoula, E. 2015, A&A, 580, A126. doi:10.1051/0004-6361/201424171
- Mackereth, J. T., Bovy, J., Leung, H. W., et al. 2019, MNRAS, 489, 176. doi:10.1093/mnras/stz1521
- Sanders, J. L. & Binney, J. 2016, MNRAS, 457, 2107.
doi:10.1093/mnras/stw106
- Haywood, M., Di Matteo, P., Lehnert, M. D., et al. 2013, A&A, 560, A109. doi:10.1051/0004-6361/201321397
- Toyouchi, D. & Chiba, M. 2014, ApJ, 788, 89.
doi:10.1088/0004-637X/788/1/89
- Mikolaitis, Š., Hill, V., Recio-Blanco, A., et al. 2014, A&A, 572, A33. doi:10.1051/0004-6361/201424093
- Aumer, M., Binney, J., & Schönrich, R. 2016, MNRAS, 462, 1697. doi:10.1093/mnras/stw1639
- van der Walt, S., Colbert, S. C., & Varoquaux, G. 2011, Computing in Science and Engineering, 13, 22.
doi:10.1109/MCSE.2011.37

- Haywood, M., Lehnert, M. D., Di Matteo, P., et al. 2016, *A&A*, 589, A66. doi:10.1051/0004-6361/201527567
- Gaia Collaboration, Brown, A. G. A., Vallenari, A., et al. 2021, *A&A*, 649, A1. doi:10.1051/0004-6361/202039657
- Ness, M., Hogg, D. W., Rix, H.-W., et al. 2016, *ApJ*, 823, 114. doi:10.3847/0004-637X/823/2/114
- Lindegren, L., Klioner, S. A., Hernández, J., et al. 2021, *A&A*, 649, A2. doi:10.1051/0004-6361/202039709
- Mackereth, J. T. & Bovy, J. 2020, *MNRAS*, 492, 3631. doi:10.1093/mnras/staa047
- Minchev, I., Steinmetz, M., Chiappini, C., et al. 2017, *ApJ*, 834, 27. doi:10.3847/1538-4357/834/1/27
- Yan, Y., Du, C., Liu, S., et al. 2019, *ApJ*, 880, 36. doi:10.3847/1538-4357/ab287d
- Schönrich, R., Binney, J., & Dehnen, W. 2010, *MNRAS*, 403, 1829. doi:10.1111/j.1365-2966.2010.16253.x
- McMillan, P. J. 2017, *MNRAS*, 465, 76. doi:10.1093/mnras/stw2759
- Oliphant, T. E. 2007, *Computing in Science and Engineering*, 9, 10. doi:10.1109/MCSE.2007.58
- Hunter, J. D. 2007, *Computing in Science and Engineering*, 9, 90. doi:10.1109/MCSE.2007.55
- Hu, G. & Shao, Z. 2022, *ApJ*, 929, 33. doi:10.3847/1538-4357/ac590e
- Lian, J., Thomas, D., Maraston, C., et al. 2020, *MNRAS*, 497, 2371. doi:10.1093/mnras/staa2078
- Spitoni, E., Silva Aguirre, V., Matteucci, F., et al. 2019, *A&A*, 623, A60. doi:10.1051/0004-6361/201834188
- Sellwood, J. A. & Binney, J. J. 2002, *MNRAS*, 336, 785. doi:10.1046/j.1365-8711.2002.05806.x
- Solway, M., Sellwood, J. A., & Schönrich, R. 2012, *MNRAS*, 422, 1363. doi:10.1111/j.1365-2966.2012.20712.x
- Roškar, R., Debattista, V. P., Quinn, T. R., et al. 2012, *MNRAS*, 426, 2089. doi:10.1111/j.1365-2966.2012.21860.x
- Schönrich, R. & Binney, J. 2009, *MNRAS*, 396, 203. doi:10.1111/j.1365-2966.2009.14750.x
- Sellwood, J. A. 2014, *Reviews of Modern Physics*, 86, 1. doi:10.1103/RevModPhys.86.1
- Holmberg, J., Nordström, B., & Andersen, J. 2009, *A&A*, 501, 941. doi:10.1051/0004-6361/200811191
- Aumer, M. & Binney, J. J. 2009, *MNRAS*, 397, 1286. doi:10.1111/j.1365-2966.2009.15053.x
- Lian, J., Thomas, D., Maraston, C., et al. 2020, *MNRAS*, 494, 2561. doi:10.1093/mnras/staa867

Table 1. Summary of parameters for thick disk stars

APOGEE-ID ^a	SOURCE-ID ^b	$[\alpha/\text{M}]$ ^c dex	$[\text{M}/\text{H}]$ ^d dex	Age ^e Gyr	$P_{h\alpha}$ ^f	L_Z kpc km s ⁻¹	L_P kpc km s ⁻¹	ecc	R_g kpc	R_{gc} kpc
2M00080293+1354102	2768636008919583488	0.155	-0.902	...	0.62	2271.86	588.26	0.14	9.00	9.89
2M00095633+6739200	528907737695674496	0.202	-0.929	4.61	0.45	558.74	442.44	0.78	10.24	2.43
2M03544189-6938299	4666648650490972800	0.199	-0.928	9.00	0.80	1033.97	231.20	0.42	7.89	4.50
2M05200684+2919227	3446462494832460672	0.207	-0.925	6.43	0.84	1457.72	434.60	0.48	11.57	6.34
2M09474458+0244510	3847051689345915648	0.226	-0.469	8.56	1.00	409.23	371.37	0.83	9.72	1.78
2M09482299+4600232	821455518049745280	0.207	-0.498	7.44	1.00	1394.64	979.77	0.38	9.77	6.06
2M09525110+3132524	745175382746994432	0.230	-0.455	...	1.00	1368.62	232.65	0.35	8.93	5.95
2M09530067+3752199	799998372538133120	0.267	-0.465	7.41	1.00	1801.05	370.35	0.39	9.64	7.83
2M18341526-1304434	4104893557043564160	0.191	-0.406	2.94	0.96	890.77	91.96	0.18	3.45	3.89
2M18344194-2914203	4048233180241935744	0.221	-0.458	4.72	1.00	155.23	231.57	0.62	2.37	0.67

NOTE—The complete table is available on the publisher website.

^a APOGEE DR17 object name.

^b Gaia EDR3 source id.

^c $[\alpha/\text{M}]$ in APOGEE DR17.

^d $[\text{M}/\text{H}]$ in APOGEE DR17.

^e Sanders & Das (2018).

^f Table 2 of Hu & Shao (2022). The membership probabilities belonging to high- α for individual sample stars.